Tomchuk, O.V.; Bulavin, L.A.; Aksenov, V.L.; Haramus, V.M.; Ivankov, O.I.; Vul, A.Y.; Dideikin, A.T.; Avdeev, M.V.:

Small-angle scattering from polydisperse particles with a diffusive surface

In: Journal of Applied Crystallography (2014) Blackwell

DOI: 10.1107/S1600576714001216

Person to contact for this submission:
Mikhail Avdeev (avd@nf.jinr.ru; phone: (+7-49621) 62-674; fax: (+7-49621) 65-484)

Small-angle scattering from polydisperse particles with diffusive surface

Oleksandr V. Tomchuk[ab], Leonid A. Bulavin[b], Viktor L. Aksenov[ca], Vasyl M. Garamus[d], Oleksandr I. Ivankov[ab], Alexander Ya. Vul'[e], Artur T. Dideikin[e] and Mikhail V. Avdeev[a]*

[a]Frank Laboratory of Neutron Physics, Joint Institute for Nuclear Research, Dubna, 141980, Russia, [b]Taras Shevchenko National University of Kyiv, Kyiv, 03022, Ukraine, [c]B.P.Konstantinov Petersburg Nuclear Physics Institute, National Research Centre "Kurchatov Institute", Gatchina, Leninradskaya Reg., Russia, [d]Helmholtz-Zentrum Geesthacht, Geesthacht, Germany, and [e]Ioffe Physical-Technical Institute, Saint Petersburg, Russia

Correspondence email: avd@nf.jinr.ru

Keywords: small-angle scattering, polydisperse systems, diffusive interface, contrast variation, detonation nanodiamonds, nanocrystallites, liquid dispersions

Synopsis

Small-angle scattering from polydisperse non-homogeneous particles with diffusive interface is considered for the case of small diffusivity. The deduced simplifications both in the analysis of polydispersity and inner structure (contrast variation) of the particles are used in the treatment of the small-angle neutron scattering data from liquid dispersions of detonation nanodiamonds.

Abstract

The particles with a diffusive surface, which is characterized by a deviation from the Porod power-law asymptotic behavior in small-angle scattering towards the exponent below –4, are considered with respect to the polydispersity problem. The case of small diffusivity is emphasized, which allows one to describe the scattering length density distribution within the spherically isotropic particles in terms of a continuous profile. This significantly simplifies the analysis of the particle size distribution function, as well as the change in the scattering invariants under contrast variation. The effect of the solvent scattering contribution on the apparent exponent value in the power-law type scattering and related restrictions in the analysis of the scattering curves are discussed. The principal features and possibilities of the developed approach are illustrated in the treatment

of the experimental small-angle neutron scattering data from liquid dispersions of detonation nanodiamonds. The obtained scattering length density profile of the particles fits well a transition of the diamond states of carbon inside the crystallites to graphite-like states at the surface and makes it possible to combine the diffusive properties of the surface with the experimental shift of the mean scattering length density of the particles as compared to that of pure diamond. The moments of the particle size distribution are derived and analyzed in terms of the lognormal approximation.

1. Introduction

Highly dispersed systems especially those developed for the practical use contain, as a rule, heterogeneous (multicomponent) and polydisperse nanoparticles. Often they form multiscale aggregate structures. All these factors complicate the interpretation of the experimental data of small-angle X-ray (SAXS) and neutron (SANS) scattering applied to such systems and give rise to the question of how far one can advance in the reliable structural characterization of complex colloids.

The analysis of the polydispersity of homogeneous particles composing clusters in dispersed systems was recently considered by Beaucage and colleagues (Beaucage *et al.*, 2004) in the frame of the unified exponential/power-law approach (Beaucage, 1996) employing the fact that in rather polydisperse systems the small-angle scattering curves show a smooth transition from the Guinier regime to the power-law asymptotics. As the main result, it was proposed to describe and compare the polydispersity of different systems by a polydispersity index (PDI), a definite combination of the parameters of the exponential/power-law expression. In addition, the experimentally found PDI of an arbitrary system can also be compared with the values formally calculated for different correlation types including those which can take place in a generalized two-phase system. The situation is more complicated if the particles are non-homogeneous and one cannot use this approach directly. Quite standard way for studying non-homogeneous nanoparticles by means of the small-angle scattering is the contrast variation technique based on the analysis of the changes in the scattering when varying the scattering length density (SLD) of the homogeneous carrier (or ‘solvent’) containing the studied nanoparticles. The classical applications of this method are referred to monodisperse objects such as proteins (e.g. Stuhrmann, 1982; Feigin & Svergun, 1987; Perkins, 1988; Stuhrmann, 1995). The extension of this method for polydisperse systems in terms of the modified contrast was recently considered (Avdeev, 2007*a*) including the contrast dependences of the scattering invariants (Guinier parameters, Porod volume), which were found to be principally different as compared to those for monodisperse particles. In some cases, such as in the case of the structural polydispersity (i.e. the variation in the inner structure with the same particle shape and size) the general expressions of this approach are significantly simplified and exhibit more transparent relations between the

experimentally determined parameters and the structural parameters of the particles including the parameters of the polydispersity function (Stuhrmann & Duee, 1975; Almgren & Garamus, 2005).

In this paper we consider a specific kind of polydisperse non-homogeneous particles whose structure, on the one hand, allows also significant simplifications of the general contrast variation approach in the small-angle scattering, and, on the other hand, makes it possible to analyze the scattering in the same manner as for polydisperse homogeneous particles (Beaucage *et al.*, 2004). The non-homogeneity of these particles is determined by their interface conventionally defined here as a 'diffusive surface'. It is close to the concept introduced by Schmidt (Schmidt, 1995) of a diffusive interface between two homogeneous phases to explain the experimentally observed deviations of the scattering from the Porod law towards lower values of the power-law exponent (< –4) at large *q*-values in reversed-phase silicas (Schmidt *et al.*, 1991*b*). The same deviations were revealed for SANS from ethanol solutions of hydrolyzed TEOS (Avdeev *et al.*, 2004). A recent example of such non-Porod asymptotic behavior of the scattering is related to the detonation nanodiamond (DND) both in powder state (Avdeev *et al.*, 2007*b*) and in liquid dispersions (Avdeev *et al.*, 2009). It should be noted that there are other types of surface diffusivity corresponding to fractal surfaces with the Porod exponent between −3 and −4 (e.g. Schmidt, 1995) and smeared interfaces of the spherical multi-shell type (Heinemann *et al.*, 2000; Foster, 2011) still satisfying the Porod law.

DND is characterized by an intrinsic non-homogeneous structure because of graphitic states of carbon at the particle surface (Raty *et al.*, 2003). In SANS experiments with the contrast variation on liquid DND dispersions (Avdeev *et al.*, 2009) the diamond-graphite spatial transition in DND was considered in terms of the 'core-shell' approximation, which explained the experimentally detected shift in the mean scattering length density (SLD) of DND as compared to the diamond density and gave about 0.5 nm thickness for the graphite shell in the particles with the total size of about 7 nm. It is, however, clear that the 'core-shell' representation cannot explain the above-mentioned deviation from the Porod law, and a 'broader' interface is to be introduced for this purpose. By assuming the spherical symmetry of such particles, the corresponding SLD profile by analogy with the early works on diffusive surface (Schmidt, 1995) should have the form:

$$\rho(r) = \begin{cases} \rho_0, & 0 < r < R - d, \\ \rho_0 \left(\dfrac{R - r}{d} \right)^{\beta}, & R - d < r < R, \end{cases} \tag{1}$$

where r is the distance from the particle center; R is the radius of the particle; d is the parameter determining the width of the transition layer at the particle surface; ρ_0 is the SLD of the homogeneous 'core' of the particle, which can be associated with the SLD of diamond. The exponent β lies between 0 and 1, thus defining the limit of the derivative $d\rho/dr \to \infty$ at $r = R$. This is a principal difference from the other types of the diffusive surfaces mentioned above, where the derivative of $\rho(r)$ at the

interface approaches zero. Specifically due to this feature, as it was shown (Schmidt, 1995), the asymptotic behavior of the small-angle scattering from the particles with the SLD profile of type (1) follows the expression:

$$I(q) = Bq^{-4+2\beta}, \tag{2a}$$

$$B \approx 2\pi n \rho_0^2 S \Gamma^2(\beta+1)/d^{2\beta}, \tag{2b}$$

where S is the particle surface area; n is the particle number density; $\Gamma(x)$ is the Euler gamma function.

It is important that the scattering curves from DND are rather smeared because of the particle polydispersity, so the exponential/power-law approach can be formally applied in their treatment (Avdeev *et al.*, 2007*b*; Avdeev *et al.*, 2009). At the same time, according to profile (1), the DND particles are non-homogeneous, which can have additional effects on the scattering especially in the contrast variation experiments. The aim of this work is to consider two indicated aspects of the analysis of the scattering (polydispersity and contrast variation) for the particles with the SLD profile (1). The general solution of this problem is difficult regarding the interpretation of the experimental scattering curves. However, in the case of small β (which takes place in practice) a number of simplifying factors can be indicated, thus making it possible to deduce relatively simple expressions for the scattering invariants, which take both the particle heterogeneity and polydispersity into account. The possibilities of the proposed approach are then discussed basing on the model scattering curves and experimental SANS curves obtained previously for the liquid DND dispersions (Avdeev *et al.*, 2009).

2. Model

SLD profiles corresponding to Eq. 1 with different parameters are shown for illustration in Fig. 1. In the case of a polydisperse system the particle radius R is distributed over some interval according to some function $f(R)$. As compared to homogeneous particles, here, the moments $\langle R^n \rangle$ depend additionally on the profile parameters d and β. This makes the expressions for the moments rather cumbersome because of the size-dependent contributions of the $\rho(r)$ function and does not allow one to use the ideas of the approach (Beaucage *et al.*, 2004). However, some principal simplifications can be considered, if one takes experimental peculiarities into account. First, for DND particles the β-parameter should be sufficiently small (which is observed in practice) to describe the transition from diamond in the center ($\rho_{diam} = 11.8(3) \times 10^{10}\,\mathrm{cm}^{-2}$) to graphite ($\rho_{graph} = 7.0(3) \times 10^{10}\,\mathrm{cm}^{-2}$) at the periphery. This case is illustrated in Fig.1 where for comparison the 'core-shell' profile corresponding to these SLDs is given. One can see that at $\beta << 1$ the profiles corresponding to Eq.1 almost coincide with the sharp 'core-shell' interface at $r = R$ because of their

infinite derivatives at the outer particle radius and, thus, describe well the transition to ρ_{graph}. The alternative way to describe this transition using (1) is to add the constant ρ_{graph} to this profile with the corresponding renormalization of the SLD of the central part. However, as it will be discussed below (see Section 4.2) such constant would affect strongly the exponent in the power-law type scattering (2*a*). The β-values obtained in the experiments on DND (see Section 6) lie around 0.1 (according to Eq.2*a* the corresponding power-law exponent of the scattering is –4.2) and satisfy well the discussed condition. The second simplification is related to the fact that while the profile (1) explains the non-Porod behavior of the scattering at large *q*-values, still when fitting it to the experimentally found mean SLD of DND (see Section 6) one obtains rather large *d*-values. Thus, for a 7-nm DND nanoparticle in the monodisperse approximation the corresponding estimates give $d = 2.5$ nm. This means that being polydisperse a significant part of the particles meets the condition $d \approx R$. This gives an idea to consider the corresponding approximation (Fig. 1) as an intrinsic property of all particles. So, the substitution $d = R$ into (1) gives the profile:

$$\rho(r) = \rho_0 \left(1 - \frac{r}{R}\right)^{\beta}, \quad 0 < r < R. \tag{3}$$

The smaller is the β -value the less is the difference between (3) and (1). So, the smallness of the β -parameter allows one to consider the profile (3) as a good approximation to (1) in the case when *d* is not strictly equal to *R* but approaches it (see Fig. 1). The made substitution has two important (from the practical viewpoint) consequences. First, the number of parameters that define the SLD profile (and, hence, the moments $\langle R^n \rangle$) is reduced. Second, the mean SLD over the particle volume becomes independent of the particle radius *R* and is determined only by the "core" SLD ρ_0 and exponent β as:

$$\overline{\rho} = \frac{3}{R^3}\int_0^R \rho(r) r^2 dr = \frac{6\rho_0}{(\beta+1)(\beta+2)(\beta+3)}. \tag{4}$$

Similarly, the size independence retains for any mean *n*-th power of $\rho(r)$ over the particle volume in such approximation:

$$\overline{\rho^n} = \frac{3}{R^3}\int_0^R \rho(r)^n r^2 dr = \frac{6\rho_0^n}{(n\beta+1)(n\beta+2)(n\beta+3)}. \tag{5}$$

3. Analysis of polydispersity using the unified exponential/power-law approach

By analogy with the work (Beaucage *et al.*, 2004) we consider first the powder state of nanoparticles with the diffusive interface (3). A similar case is when the particles are located in a weakly scattering liquid with SLD $\rho_s \sim 0$. In the frame of the unified exponential/power-law approach (Beaucage, 1996) the scattered intensity for such particles has the form:

$$I(q) = G \exp\left(-q^2 R_g^2/3\right) + B\,(q^*)^{-P}, \tag{6}$$

where the Guinier regime with the parameters G (forward scattered intensity) and R_g (radius of gyration) at small q-values is combined with the power-law scattering regime (exponent $P = 4+2\beta$) at large q-values by the renormalization of the q-variable in the power-law term as $q^* = q/[erf(qR_g/\sqrt{6})]^3$. The explicit form of the B parameter is given in Eq.2*b*.

Using the definitions of the Guinier parameters together with the SLD profile (3) and applying the averaging over the particle radius distribution function (here and below denoted by brackets $\langle \ldots \rangle$) one obtains:

$$G = n\bar{\rho}^2 (4\pi/3)^2 \left\langle R^6 \right\rangle, \tag{7a}$$

$$R_g^2 = \frac{12}{(\beta+4)(\beta+5)} \frac{\left\langle R^8 \right\rangle}{\left\langle R^6 \right\rangle}. \tag{7b}$$

One can see that the mean SLD of the particles $\bar{\rho}$ calculated according to Eq.4 is factored out in (7*a*) because it does not depend on the particle size. The corresponding averaging of the parameter B in (2*a*) and (6) results in the expression:

$$B = 8\pi^2 n \rho_0^2 \Gamma^2(\beta+1) \left\langle R^{2-2\beta} \right\rangle, \tag{8}$$

where, in addition to (2*b*), the explicit relation between S and R for the spherical particles is taken into account.

Then, one can propose a modification of the polydispersity index PDI in the given case. For the particles with the sharp boundary it is combined as a dimensionless ratio (Beaucage *et al.*, 2004)

$$\mathrm{PDI} = \frac{BR_g^4}{G}, \tag{9}$$

and takes its minimally possible value of 1.62 for homogeneous monodisperse spheres. Then, the normalized PDI index is introduced as

$$\mathrm{PDI_n} = \frac{BR_g^4}{1.62G}. \tag{10}$$

Its value (which can be obtained directly from the experimental curve) is related to a polydispersity model, so $\mathrm{PDI_n}$ can be used as a classification parameter. In the case of polydisperse particles with the diffusive surface only equation for the B-coefficient is principally modified from the viewpoint of averages of different powers of R, since it contains the average of the non-integer power of R (see Eq.8). The analog of PDI indexes in this case are the combinations:

$$\mathrm{PDI} = \frac{BR_g^{4+2\beta}}{G}, \tag{11a}$$

$$\mathrm{PDI}_n = \frac{BR_g^{4+2\beta}}{t(\beta)G}, \tag{11b}$$

where

$$t(\beta) = \frac{1}{8}(\beta+1)(\beta+2)(\beta+3)\Gamma(\beta+1)^2\left(\frac{12}{(\beta+4)(\beta+5)}\right)^{2+\beta} \sim 1.62 + 1.78\beta + 0.88\beta^2. \tag{12}$$

It should be noted that along with the polydisperse particles with diffusive surface (1) Eqs. 11 are valid also for the two-phase systems with analogous radially averaged interface $\rho(r)$ characterized by the wide diffuse transition from one phase to another. Since β is assumed to be small, still the normalized index PDI_n can be used for the evaluation of the correlation type in the system, which is responsible for the observed transition from the Guinier to the power-law scattering. Here, the particles themselves are of a spherical shape with strict boundary for the solvent, so the only appropriate model, which can be naturally considered, is the model of polydisperse particles. Then PDI_n index is to be used for comparison of the polydispersity rate in the studied systems with small β without any knowledge about the particle size distribution. As is shown in (Beaucage *et al.*, 2004), in practical analysis of small-angle scattering data it is convenient to consider the particle polydispersity in terms of the approximation of the log-normal distribution of spherical particles:

$$f(R) = \exp\left[-\ln^2(R/R_0)/2s^2\right] / Rs(2\pi)^{1/2}. \tag{13}$$

Parameters R_0 and s of the function (13) are directly determined by the PDI_n index. Here, the corresponding expressions take the form:

$$s = \sqrt{\frac{\ln \mathrm{PDI}_n}{12 + 10\beta + 2\beta^2}}, \tag{14a}$$

$$R_0 = R_g\sqrt{\frac{(\beta+4)(\beta+5)}{12\exp(14s^2)}}, \tag{14b}$$

Thus, for the SLD profile (3) the ideology of the approach (Beaucage *et al.*, 2004) in the data analysis of the small-angle scattering from spherical-like particles with diffusive surface can be applied after some renormalizations in the equations for the scattering invariants (7), (8). This means that at small β-values the effect of $\rho(r)$ on the moments $\langle R^n \rangle$ is similar to that in the case of homogeneous particles and explains the fact that the unified exponential/power-law approach can be well applied in the treatment of the experimental SANS data from non-homogeneous DND particles (Avdeev *et al.*, 2009).

It is important to note that the considered approach is not valid for the pores with diffusive surface. The presence of a matrix (solvent) with zero SLD is essential for the obtained expressions. The 'solvent-pores' inversion results in a principally different profile as compared to (1). By this reason, the scattering from DND powders, where the pores are the scattering particles against the matrix of DND crystallites (Avdeev *et al.*, 2007*b*), cannot be treated properly by the proposed way to get the information about the pore polydispersity.

4. Contrast variation

4.1. Scattering invariants

The main peculiarity of the model presented in Section 2 which is essential for the contrast variation follows from Eq.4. While the particles are non-homogeneous, still its mean SLD is size independent. Using this fact one can define the effective mean SLD in the concept of the modified contrast (Avdeev, 2007*a*) as follows:

$$\bar{\rho}_e = \langle \bar{\rho} V_c^2 \rangle / \langle V_c^2 \rangle = \bar{\rho} \,. \tag{15}$$

Here and below V_c denotes the particle volume inaccessible for the solvent, which for the SLD profile (3) equals to the volume of a sphere of radius *R*. Consequently, the contrast in the system is defined as:

$$\Delta\rho = \bar{\rho} - \rho_s \,. \tag{16}$$

Then the forward scattered intensity has the form:

$$G = n(\bar{\rho}_e - \rho_s)^2 \langle V_c^2 \rangle + n\langle (\bar{\rho} - \bar{\rho}_e)^2 V_c^2 \rangle = n(\Delta\rho)^2 \frac{16\pi^2}{9} \langle R^6 \rangle \,, \tag{17}$$

i.e. in the effective match point (minimum in the intensity as a function of the contrast) the parameter (17) takes zero value. This means that as compared to the polydisperse non-homogeneous particles in the general case there is full matching for the considered particles with diffusive surface in the approximation (3) as for monodisperse particles!

The second Guinier parameter, radius of gyration, in the case of monodisperse non-homogeneous particles depends on the contrast as:

$$R_g^2 = R_c^2 + \frac{a}{\Delta\rho} - \frac{b}{(\Delta\rho)^2} \,, \tag{18}$$

where:

$$a = V_c^{-1} \int_{V_c} (\rho(\vec{r}) - \bar{\rho}) \vec{r}^{\,2} d\vec{r} \,, \tag{19a}$$

$$b = V_c^{-2} \int_{V_c} \int_{V_c} (\rho(\vec{r}_1) - \overline{\rho})(\rho(\vec{r}_2) - \overline{\rho})(\vec{r}_1 \vec{r}_2) d\vec{r}_1 d\vec{r}_2 \,. \tag{19b}$$

Here, R_c is the radius of gyration of the particle shape related to the volume V_c (for the considered spherical particles it is $R\sqrt{3/5}$). The parameters *a* and *b* are determined by the fluctuations of SLD inside the particles and formally describe the relative location of the particle components with different SLDs. It can be stated with assurance that in the frame of the considered model of the SLD profile (3) the *a*-parameter is negative, since 'lighter' (from the viewpoint of scattering) components are at the periphery. Its direct calculation according to (19*a*) for the profile (3) gives:

$$a = \frac{3}{5} R^2 \overline{\rho} \left(\frac{20}{(\beta + 4)(\beta + 5)} - 1 \right) = -\frac{18}{5} R^2 \rho_0 v(\beta) < 0 \,, \tag{20}$$

where

$$v(\beta) = \frac{\beta(\beta + 9)}{\prod_{i=1}^{5} (\beta + i)} \,. \tag{20a}$$

For the particles with the spherically symmetric SLD profiles the *b*-parameter is certain to take zero value:

$$b = 0 \,. \tag{21}$$

For polydisperse particles in the general case in accordance with (Avdeev, 2007*a*) for R_g one has:

$$R_g^2 = \left[\frac{\langle R_c^2 V_c^2 \rangle}{\langle V_c^2 \rangle} + \frac{A}{\Delta\rho} - \frac{B}{(\Delta\rho)^2} \right] \left[1 + \frac{D}{(\Delta\rho)^2} \right]^{-1} , \tag{22}$$

where

$$A = \langle V_c^2 \rangle^{-1} \left[\langle a V_c^2 \rangle + 2 \langle (\overline{\rho} - \overline{\rho}_e) R_c^2 V_c^2 \rangle \right] , \tag{23a}$$

$$B = \langle V_c^2 \rangle^{-1} \left[\langle b V_c^2 \rangle - \langle (\overline{\rho} - \overline{\rho}_e) a V_c^2 \rangle - \langle (\overline{\rho} - \overline{\rho}_e) R_c^2 V_c^2 \rangle \right] , \tag{23b}$$

$$D = \langle V_c^2 \rangle^{-1} \langle (\overline{\rho} - \overline{\rho}_e) V_c^2 \rangle \,. \tag{23c}$$

Using (15) and substituting (23) in Eqs. (20), (21) one obtains:

$$A = \langle V_c^2 \rangle^{-1} \langle a V_c^2 \rangle = -\frac{18}{5} \frac{\langle R^8 \rangle}{\langle R^6 \rangle} \rho_0 v(\beta) < 0, \tag{24a}$$

$$B = 0 \,, \tag{24b}$$

$$D = 0 \,. \tag{24c}$$

from which:

$$R_g^2 = \frac{3}{5}\frac{\langle R^8\rangle}{\langle R^6\rangle}\left(1+\frac{\overline{\rho}}{\Delta\rho}\left(\frac{20}{(\beta+4)(\beta+5)}-1\right)\right) = \frac{3}{5}\frac{\langle R^8\rangle}{\langle\ ^6\rangle}\left(1-\frac{6\rho_0 v(\beta)}{\Delta\rho}\right). \tag{25}$$

For completeness we give the contrast changes of the inverse Porod volume for polydisperse particles, which are described by the general dependence (Avdeev, 2007*a*):

$$\frac{1}{V_p} = \left[\frac{\langle V_c\rangle}{\langle V_c^2\rangle}+\frac{E}{\Delta\rho}+\frac{F}{(\Delta\rho)^2}\right]\left[1+\frac{D}{(\Delta\rho)^2}\right]^{-1}, \tag{26}$$

where:

$$E = 2\langle V_c^2\rangle^{-1}\langle(\overline{\rho}-\overline{\rho}_e)V_c\rangle, \tag{27a}$$

$$F = \langle V_c^2\rangle^{-1}\left[\left\langle \overline{\rho^2}-\overline{\rho}^2\ \ V_c\right\rangle+\langle(\overline{\rho}-\overline{\rho}_e)^2 V_c\rangle\right]. \tag{27b}$$

In accordance with (24*c*) the *D* parameter is zero. The *F* parameter contains the average of the mean-square fluctuation of SLD inside the particle, whose calculation together with the mean SLD requires the mean value of the squared SLD. From (5) one has:

$$\overline{\rho^2} = \frac{6\rho_0^2}{(2\beta+1)(2\beta+2)(2\beta+3)}. \tag{28}$$

Then, for parameters (27) one obtains:

$$E = 0, \tag{29a}$$

$$F = \frac{3}{4\pi}\frac{\langle R^3\rangle}{\langle R^6\rangle}\ \overline{\rho^2}-\overline{\rho}^2\ > 0, \tag{29b}$$

$$D = 0. \tag{29c}$$

Similarly, the explicit expression for the inverse Porod volume for the considered particle type has the form:

$$\frac{1}{V_p} = \frac{3}{4\pi}\frac{\langle R^3\rangle}{\langle R^6\rangle}\left(1+\frac{\overline{\rho^2}-\overline{\rho}^2}{\Delta\rho^{\ 2}}\right), \tag{30}$$

4.2. Basic functions

Finally, we consider the approach of the basic functions for the particles with the SLD profile (3). According to Stuhrmann (Stuhrmann, 1995) the general form of the scattered intensity for monodisperse particles as a function of the contrast has the form:

$$I(q) = I_s(q)+\Delta\rho I_{cs}(q)+(\Delta\rho)^2 I_c(q), \tag{31}$$

where $I_c(q)$, $I_s(q)$, $I_{cs}(q)$ are the so-called basic functions which traditionally denote the 'shape scattering' (scattering at the infinite contrast), the scattering from the inhomogeneity distribution within a particle (scattering at the match point) and the interference function, respectively.

The scattered intensity for the monodisperse particles with the SLD profile (3) can be expressed as:

$$I(q) = n\ W - \rho_s V_c \Phi\ ^2, \tag{32}$$

where

$$W = 4\pi\rho_0 / q \int_0^R (1 - r/R)^{\beta} r \sin(qr) dr, \tag{33a}$$

$$\Phi = 3\ \sin(qR) - qR\cos(qR)\ /(qR)^3. \tag{33b}$$

Accordingly the basic functions take the forms:

$$I_s(q) = n(W - \overline{\rho} V_c \Phi)^2, \tag{34a}$$

$$I_{cs}(q) = 2nV_c \Phi (W - \overline{\rho} V_c \Phi), \tag{34b}$$

$$I_c(q) = nV_c{}^2 \Phi^2. \tag{34c}$$

As one can see, the asymptotic behavior of the scattered intensity at large q-values is sensitive to the absolute value of ρ_s. Thus, the form (2*b*) of the *B*-parameter is valid only at $\rho_s \sim 0$. An increase in ρ_s results in the contrast growth, and the contribution of $I_c(q)$ with the squared contrast start to prevail. This leads to deviations in the exponent of the power law (2*b*) from $-(4+2\beta)$ and finally the scattering is transformed to the Porod regime from homogeneous spheres (formally at infinite contrast). In the case of $\Delta\rho \sim 0$ (match point) the scattering is determined only by the I_s function; again, the asymptotic scattering retains the power-law form, but the corresponding exponent is now determined by the interference between *W* and Φ functions in (34*a*).

The presence of the solvent is formally equivalent to the situation when the particles with the effective SLD profile $\rho(r) - \rho_s$ are located in a vacuum. For this reason, the addition of the constant ρ_{graph} to the profile (1) to combine directly the diffusive properties of the surface and the transition to the graphite SLD at $r = R$ would disturb the power law in the same way as the solvent effect mentioned above.

When the particles are polydisperse, Eq. 31 is averaged in the way:

$$I(q) = \langle I_s(q) \rangle + \Delta\rho \langle I_{cs}(q) \rangle + (\Delta\rho)^2 \langle I_c(q) \rangle. \tag{35}$$

Here, it is taken into account that according to Eqs. 15, 16 the contrast does not depend on the particle size. In terms of the concept (Avdeev, 2007*a*) the modified basic functions for polydisperse particles

with the SLD profile (3) are equal to averaged basic functions (34) of the corresponding monodisperse particles.

So, the considered approximation to the SLD profile for the particles with diffusive surface gives comparatively simple expressions for the scattering invariants and basic functions, which takes the diffusivity index β into account.

5. Model calculations

5.1. Analysis of polydispersity

First, we consider the possibilities of the approach proposed in Section 4.1 for the model curves corresponding to polydisperse particles with the SLD profile (3). To satisfy the smallness the β-exponent is varied in following modeling in the range of 0 - 0.2. Also, we assume that the particle size distribution function is of the lognormal type with the typical parameters of nanoparticles, $R_0 = 5$ nm, $s = 0.3$. One can see that at $\rho_s = 0$ the ρ_0-value determines just the scaling factor of the scattering, so it is set unity in the calculations. A differential cross-section per particle (on the basis of Eq. 32 averaged with (13)) over a typical q-range of 0.01 - 5 nm^{-1} for both SAXS and SANS present-day instruments is presented in Fig.2. In accordance with Eq.2 the power-law decrease in the scattering is observed at large q-values with the exponent values between –4.4 and –4.0.

The model curves are then treated in two ways. First, to calculate the PDI index and characteristics of the size distribution function the scattering parameters are obtained by applying the unified exponential/power-law approximation (6) over the total q-range (Fig.2). Second, the forward scattered intensity G and radius of gyration R_g are derived from the analysis of the Guinier range, while the direct fitting of the power law to the curve at large q-values gives B and β (see inset in Fig.2). In both ways the found invariants coincide within the errors. As a result, with increasing β the PDI_n index (11*b*) changes between 3.0 (at $\beta = 0$) and 3.5 (at $\beta = 0.2$). The PDI_n-values are consequently used for determining the parameters of the particle size distribution in accordance with (14), and for all curves independently of β the values of $R_0 = 4.98$ nm, $s = 0.30$ are derived in full agreement with the model parameters.

5.2. Contrast variation

Two principally different cases of the particles with the SLD profile (3) are considered to follow the changes in the scattering curves when varying the solvent SLD in the typical interval of $(-0.5 - 6.5)\times10^{10}$ cm^{-2} restricted by the fully protonated and fully deuterated solvents in the experiments on the SANS contrast variation. Again, the polydispersity of the particles is modeled according to lognormal size distribution (13). In the first case (Model I) ρ_0 is equal to 3.0×10^{10} cm^{-2}, and the effective match point is achieved within the indicated interval of the solvent SLD. In the other

case (Model II) ρ_0 takes the value of 10.0×10^{10} cm^{-2}, which is beyond the possibly covered interval of the solvent SLD in the experiment. The other parameters are the same for the two models: $\beta = 0.1$, $R_0 = 5$ nm, $s = 0.35$, $n = 2.5\times10^{16}$ cm^{-3}. The scattering curves are calculated by Eqs. 11, 32 in a q-range of 0.03 - 5 nm^{-1}.

The scattering curves of the two models calculated for several ρ_s-values are shown in Fig.3. The parameters G and R_g are obtained from the Guinier approximation in a region of $q \leq 1/R_g$ and analyzed in Fig.4. The minima of the quadratic dependences of G on the solvent SLD (Fig.4*a*) correspond to the effective match points, which coincide well with the mean particle SLD values (calculated with Eq.4): 2.5138×10^{10} cm^{-2} against 2.5136×10^{10} cm^{-2} (Model I) and 8.3789×10^{10} cm^{-2} against 8.3787×10^{10} cm^{-2} (Model II). In full agreement with Eq.19 there is no residual scattering in the match points (see Fig.4*a*). The obtained dependences of the squared radius of gyration on the inverse contrasts in the two cases are shown in Fig.4*b*. According to (25) the linear behavior is observed for both models. The results of the fitting of Eq.22 using Eqs.24 ($B = D = 0$) are given in Table 1, where they are compared with the values calculated by using the initial model parameters. One can see that they coincide within a 2% error. The fitting lines intersect the ordinate axis at one point that in the two cases gives the parameter $\langle R_c^2 V_c^2 \rangle / \langle V_c^2 \rangle$, which is a dimensional characteristic of the particles. The difference in the slopes is due to the different values of the average SLD according to (24*a*).

The important observation concerns the changes in the apparent exponent of the power law in Fig.3 with the contrast variation. The corresponding dependences for the two models are given in Fig.5*a*. It is clearly seen that at the fixed β-values the power-law type asymptotic behavior satisfies (2*a*) only when $\rho_s = 0$, which corresponds to the situation considered by Schmidt (Schmidt *et al*., 1991*b*). In the case $\rho_s \neq 0$ there are significant deviations from (2*a*), which have some specific modulation over the contrast. When $\rho_s \to \pm\infty$ (infinite contrast) the exponents for both models tend to –4 (Porod law), which is in full accordance with the results of Section 4.2. At the match points the deviation from the Porod asymptotic limits changes its sign, so that at $\rho_s \to -\infty$ the apparent *Ps* approaches –4 from above, while at $\rho_s \to +\infty$ from below. The latter situation is very important from the experimental viewpoint because the observed values of the exponent in the power-law type scattering in this case being less than –4 can be interpreted as an indication of the fractal surface. So, a careful analysis of the power-law scattering regime from non-homogeneous particles in solutions is required, when ρ_s exceeds $\bar{\rho}$.

6. Experimental aspects: liquid dispersions of detonation nanodiamond

The systems where the considered approach can be applied to some extent are the liquid dispersions of detonation nanodiamond. DND particles are ultra-fine single crystals of cubic diamond

with diameters of 4-5 nm (according to X-ray diffraction), which are formed during an explosion of oxygen-imbalanced explosives (Poole *et al*., 2000; Roduner, 2006; Baidakova & Vul', 2007; Vul', 2013). Such particles are of current interest both from the practical and fundamental viewpoints. The latter is due to the fact that the DND particles are characterized by a natural change from sp^3 hybridization of carbon in the 3D diamond structure to a surface sp^2-hybridized graphite-like state (Raty *et al*., 2003; Eidelman *et al*., 2005). The existence of the diamond lattice in 3D even at this limiting size scale is well supported by the X-ray diffraction (XRD) data (Shenderova *et al*., 2002; Baidakova & Vul', 2007; Ōsawa, 2008; Vul', 2013). At the same time, the sp^2 hybrid bonds are reflected in various spectroscopic (UV-Raman, XANES, FTIR) (Osswald *et al*., 2006) and resonance (EPR, NMR) (Panich *et al*., 2006) methods. In some cases, a graphite-like shell comprising two-three graphene sheets is resolved directly in HRTEM images (Aleksenskii *et al*., 1999). If one takes into account a large difference in SLD of diamond and graphite (these values are used for showing core-shell SLD profile in Fig.1), then DND particles are to be considered as strongly non-homogeneous from the viewpoint of SANS, which can be applied for studying the discussed spatial transition.

DND powders are to be purified and disaggregated before the single crystals are placed in liquid media; the complete separation is properly verified by dynamic light scattering. The final dispersions are highly stable (presumably because of some charge distribution on the particle surface), which makes it possible to use the SANS contrast variation for these systems. The polyhedral nature of DND particles (Raty *et al.*, 2003; Barnard, 2008) makes it possible to consider them as spheres in small-angle scattering experiments; the spherical approximation for polyhedrons is valid for $qR_g < 8$ (Feigin & Svergun, 1987) which is the case in the experiments referenced below.

However, an extremely high specific surface area of the separated DND nanoparticles in solutions results in the new aggregate growth especially for concentrated samples with the particle fraction above 1 wt % required for SANS experiments. Here, we consider the data of such experiments obtained previously (Avdeev *et al*., 2009) for the concentrated (10 wt. %) liquid DND dispersions in water and dimethylsulphoxide (DMSO) synthesized at the NanoCarbon Research Institute (Nagano, Japan) by stirred-media milling together with powerful sonication in wet conditions (Krüger *et al*., 2005; Ōsawa, 2008), initial DND powder from Gansu Lingyun Nano-Material Co., Ltd. (Lanzhou, China). The scattering curves were obtained at the SANS-1 small-angle instrument at the FRG-1 steady-state reactor of the GKSS Research Centre (Geesthacht, Germany). The differential cross-section per sample volume (or scattered intensity) isotropic over the radial angle φ on the large-area detector was obtained as a function, $I(q)$, of the modulus of momentum transfer, $q = (4\pi/\lambda)\sin(\theta/2)$, where λ is the incident neutron wavelength and θ is the scattering angle. The measurements were carried out at a neutron wavelength of 0.81 nm (monochromatization $\Delta\lambda/\lambda$ = 10%) and a series of sample-detector distances within a range of 0.7-9.7 m to cover a q-range of 0.04-

2.3 nm^{-1}. H_2O was used to calibrate the curves on the detector efficiency. Additionally, the SANS experiment on a new series of the aqueous DND dispersion (3.6 wt. %) synthesized in the Ioffe Physical-Technical Institute RAS (St. Petersburg, Russia) according to the procedure described in (Aleksenskiy *et al.*, 2011), initial DND powder from the Federal State Unitary Enterprise "Technolog" (St. Petersburg, Russia), has been carried out on the YuMO small-angle time-of-flight diffractometer at the IBR-2 pulsed reactor, Joint Institute for Nuclear Research (Dubna, Russia). A two-detector setup with ring wire detectors were used (Kuklin *et al.*, 2005). The neutron wavelengths within a range of 0.05-0.8 nm and sample-detector distances of 4 and 16 m were used to obtain scattering curves in a q-range of 0.65-4 nm^{-1}. A vanadium standard was used for an absolute calibration of the intensity. The raw data treatment was performed by the SAS program with a smoothing mode (Soloviev *et al.*, 2003). All measurements were made in 1 mm thick quartz cells (Hellma) at room temperature.

During the SANS contrast variation experiments the initial samples based on the H-solvents were diluted twice with various mixtures of the corresponding H/D solvents (the corresponding mixtures were measured and subtracted as buffer solutions). Figure 6 represents all experimental data. The absence of secondary peaks and bands in the scattering curves reflects the polydisperse nature of the DND particles. Two scattering levels are distinguished corresponding to a particle level (large q-values) and a cluster level (small q-values). Both of them reveal the power-law-type dependences (linear behaviors in the double logarithmic scale). The found exponents of about –2.3 (Fig.6*a*, *b*) and –2.5 (Fig.6*c*) for the cluster level show that the clusters are mass fractals (Schmidt, 1991*a*). The influence of the structure-factor corresponding to the cluster-cluster interaction results in an effective Guinier-type regime at smallest q-values, which makes it possible to estimate the apparent radius of gyration of the clusters. The comparatively high absolute scattered intensities observed at this level can give rise to the question about the possible multiple scattering. However, one can see that with increasing volume fraction of a deuterated component in a solvent, η, the curves at this level differ just by some scaling factors (up to 2.5), i.e. the character of the curves remains the same. This proves that the multiple scattering effect is negligibly small within the experimental errors. The particle level gives the exponent of about –4.14 (Fig.6*a*, *b*) and –4.12 (Fig.6*c*) corresponding to the particles with the diffusive surface in accordance with Eq.2*a*. The fact that the smoothed character of both levels retains at the contrast variation allows one to apply the exponential/power-law approximation (6) to the curves with different η-values, but it should be extended for the two levels as follows (Beaucage, 1996):

$$I(q) = G \exp\left(-q^2 R_g^2/3\right) + B \exp\left(-q^2 R_{gND}^2/3\right) q^{*\,-P} + \\ + G_{ND} \exp\left(-q^2 R_{gND}^2/3\right) + B_{ND} \left(q_{ND}^*\right)^{-Ps} + C \,. \qquad (36)$$

Here, the '*ND*'-index denotes the particle (nanodiamond) level; *Ps* corresponds to the particle surface; parameters without indexes correspond to the cluster level; renormalizations q^*, q^*_{ND} are made with R_g, R_{gND}, respectively. Also, Eq. 36 contains the residual incoherent scattering background, *C*, usually occurred in neutron scattering experiments. When fitting the SANS data all parameters in Eq.36 were varied independently to avoid possible artifacts because of constraints (Hammouda, 2010). The resulting fits of (36) are given in Fig.6. One can see that the scattering at the cluster level complicates the direct interpretation of the curves according to the equations given in sections 3, 4, which can be used now with some restrictions.

As follows from the note in section 3, the analysis of the polydispersity can be made only for the solutions with $\rho_s = 0$. The closest cases from the experimental solutions to this condition are the solutions with 10% of D_2O ($\rho_s = 0.13\times10^{10}\,\mathrm{cm}^{-2}$) and 0% of D-DMSO ($\rho_s = -0.046\times10^{10}\,\mathrm{cm}^{-2}$), respectively. The found parameters of the particle level from the corresponding scattering curves are collected in Table 2 together with the determined parameters of diffusivity β and PDI_n indexes (in accordance with Eq. 11*b*). Using the experimental parameters and the calculated PDI_n indexes, one obtains (in accordance with Eqs.14) the parameters of the particle size distribution function in the log-normal approximation (R_0, *s*) and the corresponding calculated mean radii and standard deviations ($\langle R\rangle$, σ), which are also presented in Table 2. Their values reflect well the fact that the DND particles are strongly polydisperse. The rate of the polydispersity differs for the systems from different producers, which follows from the comparison of the PDI_n indexes as well as from the parameters of the effective log-normal distribution. The corresponding mean diameter of the particles, ~3 nm, is less than the characteristic size determined by X-ray diffraction (4.5 nm). In the last method the coherent scattering region, *L*, is defined from the peak broadening according to the Scherrer formula (Balzar *et al*., 2004):

$$L = \frac{\lambda}{B(2\theta)\cos(\theta)}, \tag{37}$$

where λ is the radiation wavelength; $B(2\theta)$ is the integral peak width; and 2θ is the scattering angle. For polydisperse crystallites *L* is determined by the ratio of the fourth and third moments of the size distribution function in the way (Scardi & Leoni, 2001):

$$L = \frac{2\langle R^4\rangle}{K_B\langle R^3\rangle}, \tag{38}$$

where K_B is the Scherrer constant, which depends on the crystallite shape and type of the crystalline lattice (Palosz *et al*., 2007) and lies in the range of 0.82–1.3 (Langford & Wilson, 1978). Thus, one has the following relation between the sizes obtained with different diffraction methods:

$$2\langle R\rangle < L_{XRD} < 2(R_g)_{SANS} \sim 2\sqrt{\langle R^8\rangle/\langle R^6\rangle}. \quad (39)$$

According to the equations of section 4.1 the analysis of the contrast variation should be given for the parameters G_{ND}, R_{gND}. We found, however, that because of the effects of the cluster organization and the residual incoherent background the precision of these parameters is not sufficient to make reliable conclusions from their changes with the solvent SLD. Nevertheless, the mean particle SLD can be reliably estimated by using the cluster level, if one takes into account the fact that the branched aggregates form after the separated DND particles are dispersed in liquids. Thus, there is full access of the solvent to the particle surface (besides their contacts in the aggregates) and the formation of the voids free of the solvent ($\rho = 0$) is excluded. In this case, both the structure-factor of the particle correlation in the clusters (fractal power-law dependence) and the structure-factor corresponding to the cluster-cluster interaction (deviation from the power law at smallest q-values) are modulated by the particle form-factor dependent on the contrast. So, at one particle concentration (i.e. with one structure-factor for all solutions) the ρ_s-dependence of the scattering at the cluster level is the same as for the particle level. Here, it is analyzed by using the parameters G and R_g in Eq. 36 of the effective Guinier approximation to the initial parts of the curves. The main goal was to extrapolate the scattering to the forward scattered intensity G, which is required to find the match point. While in the general case the Guinier approximation is not so appropriate for the scattering from the interacting clusters with respect to the apparent radius of gyration, R_g, and there can be a significant systematic error in this parameter, still it does not show any change with the contrast within the experimental errors for the curves in Fig.7. Its experimentally found values are R_g = 18.3(1) nm and R_g = 17.9(2) nm (DND in water of both series, respectively) and R_g = 16.1(3) nm (DND in DMSO) in the solutions with different ρ_s. This means that the structure-factor is certainly independent of the contrast, and the G parameter depends on ρ_s in the same manner as G_{ND}. One can use it well for determination of the particle match point, and, since $G/G_{ND} \sim 100$, avoid any possible uncertainties related to the signal/background ratio.

The dependences $G^{1/2} \sim \rho_s$ are shown in Fig.7 and give the mean SLD values $\bar{\rho} = 10.5(5)\times10^{10}\,\mathrm{cm}^{-2}$ and $\bar{\rho} = 10.8(6)\times10^{10}\,\mathrm{cm}^{-2}$ (DND in water of the two series, respectively) and $\bar{\rho} = 10.2(4)\times10^{10}\,\mathrm{cm}^{-2}$ (DND in DMSO), which agree very well with the values $\bar{\rho} = 10.4(3)\times10^{10}\,\mathrm{cm}^{-2}$ and $\bar{\rho} = 10.6(5)\times10^{10}\,\mathrm{cm}^{-2}$ estimated from (4) by using the known SLD of diamond, $\rho_0 = 11.8(3)\times10^{10}\,\mathrm{cm}^{-2}$, as revealed from its crystalline structure, and experimentally found β. It is worth noting that if we use the ρ_s-dependence of the B-parameter in (36) like for G the corresponding values of the mean SLD are very close to those obtained above, namely,

$\overline{\rho} = 10.7(5) \times 10^{10}\,\mathrm{cm}^{-2}$ and $\overline{\rho} = 10.9(7) \times 10^{10}\,\mathrm{cm}^{-2}$ (DND in water of the two series, respectively) and $\overline{\rho} = 10.4(4) \times 10^{10}\,\mathrm{cm}^{-2}$ (DND in DMSO).

Thus, one has very good consistency of the continuous profile (3) reflecting the diffusive character of the particle surface with the mean particle SLD, which is not reasonably achieved, if one uses the 'core-shell' approximation. The fact that the experimental curves are obtained at ρ_s lying at one side of the match points explains the low sensitivity of the R_{gND} parameter to the contrast; it lays within 3.0-3.4 nm and has the experimental error of about 0.5 nm for all solutions. To illustrate this point, in Fig.4*a* along with the model dependences of $R_{gND} \sim 1/\Delta\rho$ the interval of the inverse contrast covered in the discussed experiments is indicated. One can see that the relative change of R_{gND} within this interval does not exceed several percent, which is within the experimental error. A widening of this interval towards lower $\Delta\rho$ will result in the growth of the background effect and, as a consequence, larger errors in R_{gND}. The similar situation takes place for the ρ_s dependence of the experimental parameter *Ps* shown in Fig.5*b*. It is reliably determined only in the vicinity of $\rho_s = 0$ and qualitatively repeats the results of the analysis of the model curves in Fig.5*a*.

It should also be pointed out that as one can see, the aggregate level in DND solutions of different origins is rather reproducible with respect to the structural characteristics. Especially it concerns the observed fractal dimension of the aggregates, which suggests one mechanism of the cluster growth in this kind of systems.

7. Conclusions

The smallness of the diffusivity exponent, β, for the particles with diffusive interface makes it possible to introduce the continuous SLD profile within the particles and principally simplify the interpretation of the scattering data from polydisperse systems. Especially it concerns the SANS contrast variation experiments with H/D substitution, where the behavior of the scattering from such particles in solutions is similar to that from monodisperse non-homogeneous particles with some effective mean SLD. As a consequence, the scattering invariants show comparatively simple and transparent contrast dependences. Nevertheless, the effect of the additional coherent scattering from the solvent is significant for the observed power-law behavior with respect to the apparent exponent, and, hence, the region when this type of the scattering can be reliably analyzed is restricted by the vicinity of $\rho_s \sim 0$. Here, the analysis of polydispersity (as for homogeneous particles) can be additionally done in terms of the concept of the modified polydispersity index.

The developed approach has been successfully probed in the structural characterization of liquid dispersions of detonation nanodiamonds, which show a deviation from the Porod law in SANS

towards the power-law-type scattering from diffusive interfaces. Again, the smallness of the experimentally observed β-parameter for DND fits well a spatial transition from bulk diamond to surface graphite states of carbon within the nanoparticles, thus justifying the use of the continuous SLD profile in the analysis of the SANS data. As a result, the size characteristics of the DND nanoparticles including the size distribution function have been obtained. A strong and developed aggregation of the DND nanoparticles in concentrated solutions makes it possible to perform the contrast variation experiments with high precision against the residual incoherent background in SANS experiments. This analysis testifies strongly in favor of the concept of the continuous profile in DND and combines the diffusive properties of the particles and the shift of the mean particle SLD from diamond SLD detected by SANS, which cannot be done in the frame of the core-shell approximation.

Table 1 Comparison of parameters of the functions $R_g^2(1/\Delta\rho)$ obtained from the calculations using the initial model parameters (calc) and from the treatment of the model scattering curves (scat).

	$\langle R_c^2 V_c^2 \rangle / \langle V_c^2 \rangle$, nm^2		A, $\times 10^{-4}$	
	calc	scat	calc	scat
Model I	83.350	83,013	-9.118	-9.062
Model II	83.350	83.29	-30,39	-30.18

Table 2 Best parameters of the particle level (G_{ND}, R_{gND}, B_{ND}, Ps) in Eq.36 fitted to the experimental curves at $\rho_s \sim 0$ and the characteristics of DND calculated using these parameters.

Sample	G_{ND}, cm^{-1}	R_{gND}, nm	B_{ND}	Ps	β	PDI$_n$	R_0, nm	s	$\langle R \rangle$, nm	σ, nm
DND in water (Fig.6*a*)	5.7(2)	3.19(4)	0.628(4)	4.14(2)	0.07(1)	7.6(5)	1.36(5)	0.40(1)	1.48(6)	0.62(3)
DND in DMSO (Fig.6*b*)	6.8(2)	3.10(2)	0.756(2)	4.14(2)	0.07(1)	6.9(3)	1.41(3)	0.40(1)	1.52(4)	0.61(2)
DND in water, new series (Fig.6*c*)	3.9(5)	3.30(8)	0.423(9)	4.12(4)	0.06(2)	9(1)	1.2(1)	0.43(2)	1.3(1)	0.58(6)

Figures

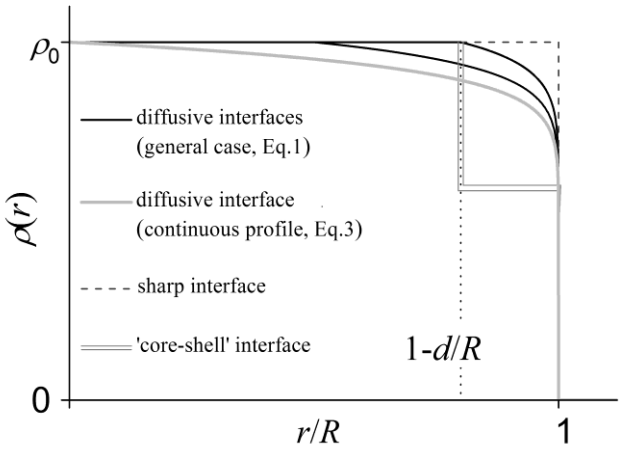

Figure 1 SLD profiles $\rho(r)$ of spherical particles (outer radius R restricts the solvent inaccessible volume) with diffusive boundary of different thickness d are compared with 'sharp' Porod and 'core-shell' interfaces. β = 0.07 << 1. ρ_0 corresponds to SLD of diamond. The SLD of the shell in the 'core-shell' approximation corresponds to the SLD of graphite.

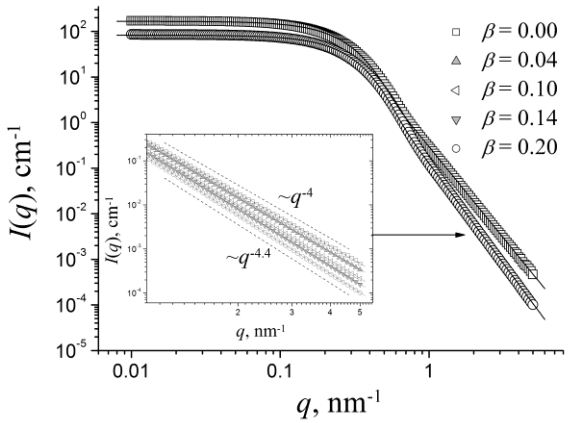

Figure 2 Model scattering curves (points) from polydisperse particles with diffusive interface (3) at ρ_s = 0 when varying β-exponent. The solid lines reflect the unified exponential/power-law approximation (6). For convenience two curves for different β-values are shown. The inset shows a power-law decrease at large q-values for several β-values with restricting curves (dashed lines) corresponding to the minimal and maximal exponent in the power-law for the considered β-interval.

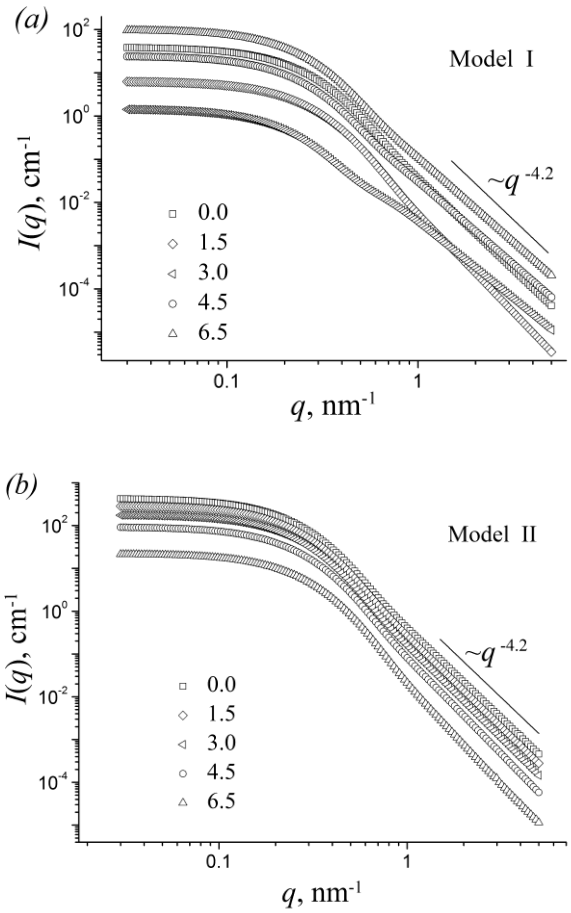

Figure 3 Changes in the scattering curves for Model I (*a*) and Model II (*b*), with the contrast variation (see text). The legends show the solvent SLDs indicated in units of 10^{10} cm^{-2}. The solid lines follow the power law corresponding to Eq.2*a*.

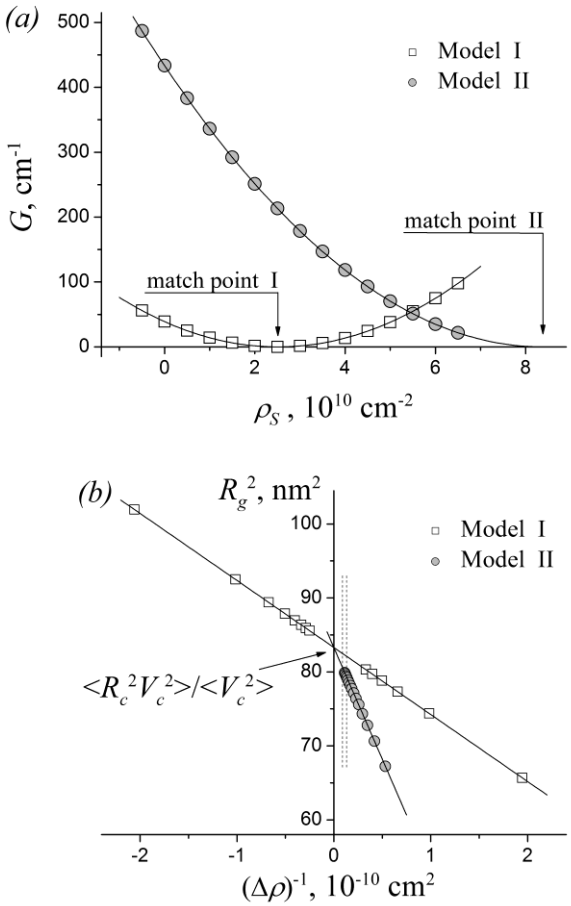

Figure 4 Guinier parameters under model contrast variation. (*a*) Forward scattered intensity as a function of the solvent SLD (points) approximated by Eq.18 (solid lines) for the two models. The found match points (shown by arrows) are used as $\overline{\rho}$ for definition of the contrast in the corresponding cases. (*b*) Squared radius of gyration as a function of the inverse contrast (points) approximated by Eq.22 using Eqs.24 (solid lines) for the two models. The vertical dashed lines restrict the interval covered in SANS experiments (Section 6).

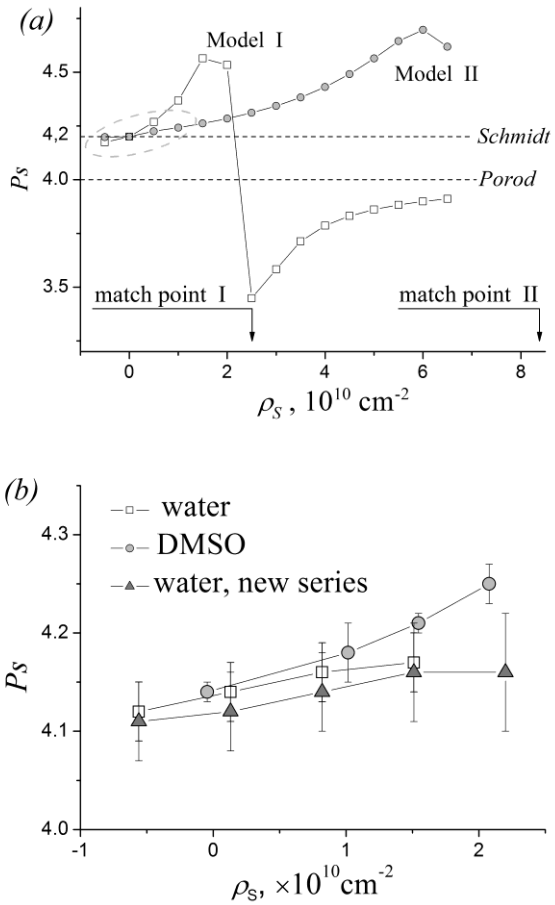

Figure 5 (*a*) Parameter *Ps* (found from the model curves) as a function of the solvent SLD for the two considered models at the same $\beta = 0.1$. The two-side arrow marks the only case ($\rho_s = 0$) when $Ps = 4+2\beta$ (Schmidt asymptotic limit). The dashed-line circle shows the region covered in SANS experiments (SANS). The one-side arrows mark the match points of the models. (*b*) Experimentally found dependences of *Ps*-parameter on the solvent SLD for the two kinds of solutions in the vicinity $\rho_s \sim 0$.

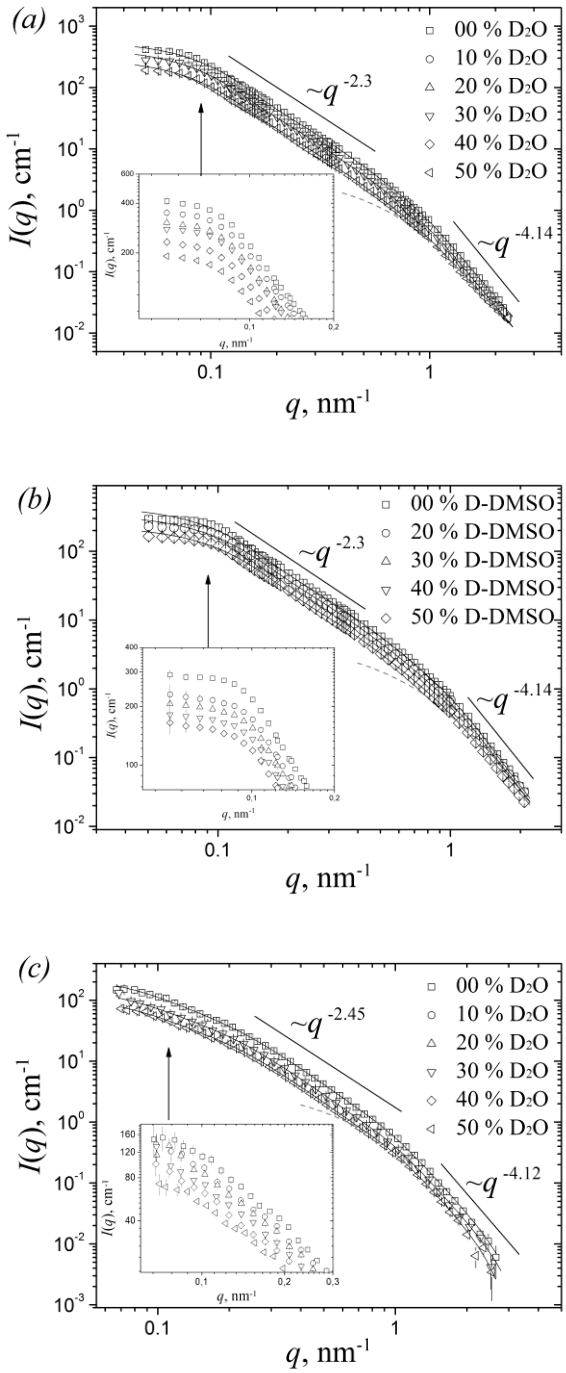

Figure 6 Experimental SANS curves for 5% DND dispersions in water (*a*) and DMSO (*b*) and 1.8 % DND dispersion in water of the new series (*c*) at different contents of the deuterated component in the solvents. For convenience three curves for each of the systems are presented. The inset contains the initial parts of all measured curves. The fitting solid lines correspond to Eq.36. The power-law behaviors for the cluster level (small *q*-values) and particle level (large *q*-values) are distinguished. As an example, the exponential/power-law approximation to the particle scattering level is shown (dashed line) for the lowest curves.

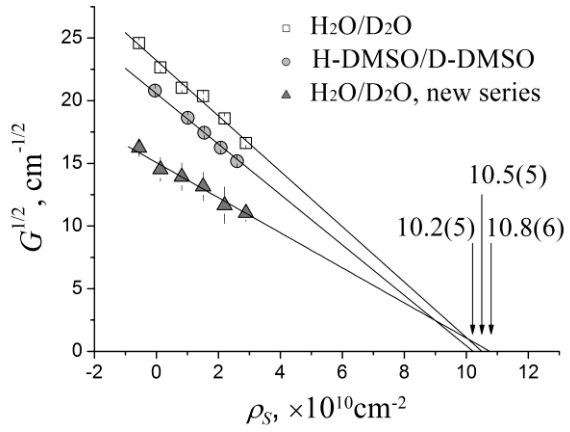

Figure 7 Experimental dependences $G^{1/2} \sim \rho_s$ for the considered solutions. Found match points are indicated in units of 10^{10} cm^{-2}.

Acknowledgements The financial support of RFBR (grant № 12-02-00649-a) is acknowledged. A.Vul' and A.Dideikin thank RFBR (grant № 12-03-12020/12) for partial support.

References

Aleksenskii, A.E., Baidakova, M.V., Vul' & A.Y. & Siklitskii, V.I. (1999). *Phys. Solid State* **41**, 668-671.

Aleksenskiy, A.E., Eydelman, E.D. & Vul', A.Ya. (2011) *Nanosci. Nanotechnol. Lett.* **3**, 68-74.

Almgren, M. & Garamus, V. M. (2005). *J. Phys. Chem. B* **109**, 11348-11353.

Avdeev, M.V., Aksenov, V.L., Kohlbrecher, J. & Rosta, L. (2004) *Physica B* **350**, E905-E908.

Avdeev, M.V. (2007*a*). *J. Appl. Cryst.* **40**, 56-70.

Avdeev, M.V., Aksenov, V.L. & Rosta, L. (2007*b*). *Diamond and Related Mater.* **16**, 2050-2053.

Avdeev, M.V., Rozhkova, N.N., Aksenov, V.L., Garamus, V.M., Willumeit, R & Ōsawa, E. (2009) *J. Phys. Chem. C.* **133**, 9473–9479.

Baidakova, M. & Vul', A. (2007) *J. Phys. D* **40**, 6300-6311.

Balzar, D., Audebrand, N., Daymond, M.R., Fitch, A, Hewat, A, Langford, J.I., Le Bail, A., Louër, D., Masson, O., McCowan, C.N., Popa, N.C., Stephens, P.W. & Toby, B.H. (2004). *J. Appl. Cryst.* **37**, 911-924.

Barnard, A.S. (2008) *J. Mater. Chem.* **18**, 4038–4041.

Beaucage, G., Kammler, H.K. & Pratsinis, S.E. (2004). *J. Appl. Cryst.* **37**, 523-535.

Beaucage, G. (1996). *J Appl. Cryst.* **29**, 134-149.

Eidelman, E.D., Siklitsky, V.I., Sharonova, L.V., Yagovkina, M.A., Vul', A.Y., Takahashi, M., Inakuma, M., Ozawa, M. & Ōsawa, E. (2005) *Diamond Related Mater.* **14**, 1765-1769.

Feigin, L. A. & Svergun, D. I. (1987). *Structure Analysis by Small-Angle X-Ray and Neutron Scattering*. New York: Plenum Press.

Foster, T. (2011) *J. Phys. Chem. B* **115**, 10207-10217.

Hammouda B. (2010) *J. Appl. Cryst.* **43**, 1474-1478.

Heinemann, A., Hermann, H., Wiedenmann, A., Mattern, N. & Wetzig, K. (2000) *J. Appl. Cryst.* **33**, 1386–1392.

Krüger, A., Kataoka, F., Ozawa, M., Fujino, T., Suzuki, Y., Aleksenskii, A.E., Vul', A.Y. & Ōsawa, E. (2005) *Carbon* **43**, 1722-1730.

Kuklin, A.I., Islamov, A.Kh. & Gordeliy, V.I. (2005) *Neutron News* **16**, 16-20.

Langford, J.I. & Wilson, A.J.C. (1978). *J. Appl. Cryst.* **11**, 102-113.

Ōsawa, E., (2008). *Pure Appl. Chem.* **80**, 1365-1379.

Osswald, S., Yushin, G., Mochalin, V., Kucheyev, S.O. & Gogotsi, Y. (2006). *J. Am. Chem. Soc.* **128**, 11635-11642.

Palosz, B., Stelmakh, S., Grzanka, E., Gierlotka, S. & Palosz, W. (2007). *Zeitschrift fur Kristallographie* **222**, 580-594.

Panich, A.M., Shames, A.I., Vieth, H.-M., Takahashi, M., Ōsawa, E. & Vul', A.Y. (2006) *Eur. Phys. J. B* **52**, 397-402.

Perkins, S. (1988). *Biochem. J.* **254**, 313-327.

Poole, Ch.P.,Frank, Jr. & Owens, J. (2000). Editors. *Introduction to nanotechnology*. 3rd edition. New York: Wiley-Interscience.

Raty, J.Y., Galli, G., Bostedt, C., Buuren, T.W. & Terminello, L.J. (2003). *Phys. Rev. Lett.* **90**, 037401.

Roduner, E. (2006) *Chem. Soc. Rev.* **35**, 583-592.

Scardi, P. & Leoni, M. (2001). *Acta Cryst.* **A57**, 604-613.

Soloviev, A.G., Solovieva, T.M., Stadnik, A.V., Islamov, A.H., & Kuklin, A.I. (2003) *JINR Communication* P10-2003-86, JINR: Dubna.

Stuhrmann, H.B. & Duee, E.D. (1975). *J. Appl. Cryst.* **8**, 538-542.

Stuhrmann, H.B. (1982). *Small-angle X-ray scattering*, edited by O. Glatter & O. Kratky, pp. 197-213, London: Academic Press.

Stuhrmann, H.B. (1995). *Modern aspects of small-angle scattering*, edited by H. Brumberger, pp. 221-254. Dordrecht: Kluwer Academic Publishers.

Schmidt, P.W. (1991*a*) *J. Appl. Cryst.* **24**, 414-435.

Schmidt, P.W., Avnir, D., Levy, D., Hörn, A., Steiner, M. & Röll, A. (1991*b*) *J. Chem. Phys.* **94**, 1474-1479.

Schmidt, P.W. (1995). *Modern aspects of small-angle scattering*, edited by H. Brumberger, pp. 1-56. Dordrecht: Kluwer Academic Publishers.

Shenderova, O.A., Zhirnov, V.V. & Brenner, D.W. (2002). *Crit. Rev. Solid State Mater. Sci.* **27**, 227-356.

Vul', A., Baidakova, M., & Dideikin, A. (2013) *Carbon Nanomaterials, Second Edition Series: Advanced Materials and Technologies*, edited by Y.Gogotsi & V. Presser, pp. 251 – 278. CRC Press.